Yttrium Oxide Upconverting Phosphors. 5. Upconversion Luminescent Emission from Holmium-Doped Yttrium Oxide under 632.8 nm Light Excitation

J. Silver,* E. Barrett, P. J. Marsh, and R. Withnall*

Centre for Phosphors and Display Materials, University of Greenwich, Chatham Maritime Campus, Chatham, Kent ME4 4TB, United Kingdom

Received: January 21, 2003; In Final Form: June 13, 2003

Both the anti-Stokes and Stokes emission properties of cubic Y_2O_3:Ho^{3+} arising from excitation at a wavelength of 632.8 nm are reported over the concentration range 0.25−10 mol % Ho^{3+}. Power dependence studies are used to assign the bands in the emission spectra. The most efficient yellow-green upconversion emission was observed at a Ho^{3+} concentration of 0.5 mol %. This originates from an absorption process involving two photons and undergoes progressive quenching as the Ho^{3+} concentration is increased. It is shown herein that as the concentration of Ho^{3+} is increased, cross-relaxation processes become dominant. These processes involving Ho^{3+} ions in the $^5F_5$ levels and the metastable $^5I_7$ states enable an alternative process for the population of the $^3K_8$, $^5F_3$, and $^5F_2$ levels that gives rise to enhanced emission between 480 and 505 nm as the concentration of Ho^{3+} ions is increased from 0.5 to 10 mol %. This cross-relaxation process is discussed in the text. In this work we also report the first discrimination between emission bands due to transitions originating from the $^5F_4$ and $^5S_2$ levels of Ho^{3+}. The emission bands originating from the $^5F_4$ level (viz. the yellow-green 530−570 nm and the near-infrared 740−780 nm bands) are shown (as expected) to have a similar dependence on the incident photon flux.

1. Introduction

As a continuation of our systematic studies[1−4] on the anti-Stokes luminescence properties of spherical phosphor particles (around 300 nm, made up of nanocrystallites in the size range 20−50 nm) of cubic Y_2O_3:M^{3+} (where M^{3+} is the trivalent cation of a rare earth element), under red laser light (632.8 nm wavelength) excitation we report here our findings for $M^{3+} = Ho^{3+}$. The reason we are studying the properties of cubic Y_2O_3:M^{3+} compounds is that we have developed a number of methods of homogeneously precipitating the phosphor precursors (to ensure atomic mixing) and controlling particle and crystallite sizes.[5−10] Furthermore, this phosphor lattice is very stable and we believe that because of the homogeneity of the dopant species, we can provide a good model for looking at interactions between evenly distributed activator ions. When M^{3+} was Eu^{3+}, the 632.8 nm (equivalent to a wavenumber of 15 803 cm^{-1}) light had insufficient energy to directly promote a transition from the ground states to the excited states (i.e., the $^5D_0$ state of Eu^{3+}).[3] However in this case the excited state could be accessed thermally.[3]

When M^{3+} was Er^{3+} or Tm^{3+}, the red laser light (15 803 cm^{-1} wavenumber) promotes the rare earth element cation directly to the $^4F_{9/2}$ or $^3F_2$ excited states respectively, closely coinciding in energy with that of the incident light.[1,2,4] In both cases the anti-Stokes properties were fairly straightforward to understand and both required the absorption of two red (632.8 nm) photons to explain these properties.

In the case of Ho^{3+} reported in this work the red laser light can promote the ion from its $^5I_8$ ground state directly to the $^5F_5$ excited state but the anti-Stokes properties are found to be more complicated and, in part, dependent on the presence of neighboring Ho^{3+} cations. In the past, Pouradier and Auzel[11] also used 632.8 nm red laser excitation to look at $Y_{1-x}Ho_xF_3$ and they put forward two possible mechanisms to account for the population of the $^5F_3$ excited state. The first of these is the absorption of a photon of 632.8 nm by a Ho^{3+} ion in the $^5I_7$ excited state (the $^5I_7$ level was previously populated by degradation of the $^5F_5$ state (populated by the 632.8 nm red laser line from $^5I_8$ to $^5F_5$)): $^5F_5 \rightsquigarrow {}^5I_4 \rightsquigarrow {}^5I_5$. The energy then passes directly to $^5I_7$ without going via the $^5I_6$ state so that the $^5F_3$ state becomes populated on absorption of a 632.8 nm photon by the Ho^{3+} ion in this state. In the course of the $^5I_5$ to $^5I_7$ transition the Ho^{3+} ion gives out 6100 cm^{-1} light (1650 nm). Alternatively, the process may involve two Ho^{3+} centers, one excited in the $^5I_5$ state and the other in its $^5I_8$ ground state so that the following scheme is followed:

$$^5I_5 + {}^5I_8 \rightarrow {}^5I_7 + {}^5I_7 + 1100\ cm^{-1}$$

Again, once the $^5I_7$ state is populated a second red photon can be accepted to populate the $^5F_3$ state.

The other way of populating the $^5F_3$ state is by additon of the energies of a Ho^{3+} ion in the $^5I_7$ state and a Ho^{3+} ion in the $^5F_5$ state according to the following scheme:

$$^5F_5 + {}^5I_7 \rightarrow {}^5F_3 + {}^5I_8$$

From their studies Pouradier and Auzel[11] concluded that the two processes could be differentiated by the influence of the Ho^{3+} ion concentration on the fluorescence. As the first mechanism is the phenomenon of a single ion and thus it has a linear dependence on Ho^{3+} ion concentration, whereas the second (which involves two Ho^{3+} ions) follows a quadratic law. They showed that the latter was correct for Ho^{3+} in $Y_{1-x}Ho_xF_3$ (where x is in the range 0−0.15).[11]

* Corresponding authors. E-mail: j.silver@gre.ac.uk, r.withnall@gre.ac.uk. Fax: 44 208 331 8405.

10.1021/jp034160j CCC: $25.00
Published on Web 07/29/2003

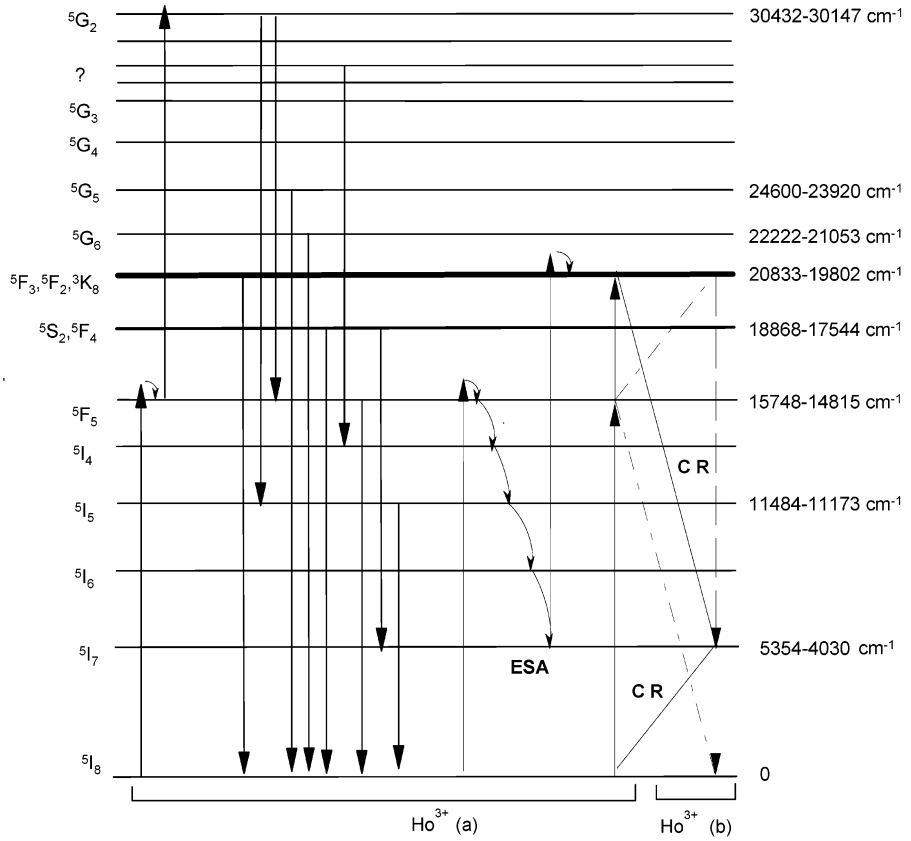

Figure 1. Schematic energy level diagram for Ho^{3+} ions in cubic Y_2O_3. The values of the energies of the levels above the ground state are derived in this work. The solid vertical lines on the left-hand side of the diagram indicate the emissions recorded in this work. The emitting levels that have not been referred to in the text are populated either by radiationless decay from higher levels or a combination of radiative and radiationless decays where the energy of the radiative part is below our detection limit. The given state labels are taken from the literature and the question mark is included because an observed transition has been ascribed to originating from it in this work. The population of the $^5G_2$ state via an ESA process is shown on the far left of the diagram. The two possible mechanisms that explain the population of the $^5F_2$, $^5F_3$, and $^3K_8$ states as a function of concentration are shown on the right-hand side of the diagram. The first of these is an ESA mechanism that gives rise to the population at lower concentrations and the second is the cross-relaxation that gives rise to the emission at higher concentrations.

Ho^{3+} is of particular interest for its role in upconversion lasers. Indeed, in 1971 the first upconversion laser was a BaY_2F_8 crystal doped with Ho^{3+} and Yb^{3+} ions and pumped by a filtered flashlamp.[12] In recent years upconversion lasing in Ho^{3+} has been described by a number of authors.[13−15] Other methods of upconversion mechanisms have also been studied for Ho^{3+} doped materials, in particular photon avalanche is one of the most efficient and complicated. It combines two phenomena, namely excited-state absorption (ESA) and cross-relaxation.[16,17] Photon avalanche has been observed in singly doped Ho^{3+} lattices.[18−22] These reports have stimulated spectroscopic investigations of Ho^{3+} in a number of host lattices for the purpose of ascertaining the properties necessary for laser action in the green region.[23−25] Measurements of upconversion energy transfer between Ho^{3+} ions in YAG ($Y_3Al_5O_{12}$) have been reported[26] and only a small number of other papers refer to upconversion processes in Ho^{3+} singly doped materials.[27−36]

2. Experimental Section

2.1. Chemical Preparation. The chemicals described throughout this section are yttrium oxide (99.99%) (Rhone Poulenc, France), holmium oxide (99.99%) (J. Matthey), urea, and nitric acid (BDH AnalaR).

The urea homogeneous precipitation method[5−10,37,38] was used to prepare spherical Y_2O_3:Ho^{3+} hydroxycarbonate submicrometer phosphor precursor powders.

Yttrium nitrate stock solution (56.4 g/L, solution A)) was prepared by dissolving Y_2O_3 in dilute nitric acid until the solution reached a pH of 3. An aqueous solution (solution B) of holmium nitrate (concentration 0.01 mole/L) was prepared from holmium oxide and nitric acid. Aliquots of solution B in the range 1.6−62.5 mL were added to 25 mL of the $Y(NO_3)_3$ stock solution (solution A). Urea (15 g) was then added, and the solution was made up to 500 mL with deionized water. The solution was kept boiling on a hot plate until turbidity was observed, then it was left for 1 h. The precipitates were filtered and washed twice with deionized water. They were then dried at 60 °C, giving soft, white powders that were converted to the oxide by firing at 980 °C for 15 h.

2.2. Characterization of Physical Properties. The morphologies and the particle sizes of the samples were determined by scanning electron microscopy (SEM) using a Cambridge Instruments, Stereoscan 90, and transmission electron microscopy (TEM) using a JEOL JEM-200CX. The average diameter (and its deviation) of the spherical particles was estimated from measuring ∼50 particles per picture.

Luminescence and Raman spectra were obtained using a Labram Raman spectrometer equipped with 1800 and 600 g/mm holographic gratings, a holographic supernotch filter and a Peltier-cooled CCD detector. Samples were excited using a helium−neon laser with an output of 8 mW of power at the sample on the 632.8 nm line, unless an attenuation filter was used.

3. Results and Discussion

3.1. Structural Investigations. SEM micrographs showed that the unfired particles of the amorphous material had diameters in the range 280−330 nm and had an appearance similar to those of other rare earth doped precursors of cubic Y_2O_3 that we have presented previously.[1,3,4] A typical TEM micrograph of fired particles of cubic Y_2O_3:Ho^{3+} showed that these were similar to those of other rare earth doped cubic Y_2O_3 materials we have presented before with crystallite sizes in the 20−50 nm range.[1,3,4] XRD powder diffraction data confirmed all the Y_2O_3:Ho^{3+} materials were cubic.

3.2. General Observations on the Spectra. The discussion below is based on observations of cubic Y_2O_3:Ho^{3+} samples, where the Ho^{3+} concentration is given in the figure captions. The Dieke energy level diagram for Ho^{3+} is given in Figure 1 in modified form with possible mechanisms involved in the anti-Stokes processes shown, and the transitions we have included on it will be used in the following discussion. The emission spectrum of cubic Y_2O_3:Ho^{3+} is presented in Figure 2a−c (for the anti-Stokes bands in the range 400−628 nm) and Figure 3a,b (for the Stokes bands in the range 635−895 nm).

Figure 2a presents a lower resolution spectrum of the bands in the 400−525 nm range, whereas Figure 2b shows the 450−525 nm bands at higher resolution.

3.3. Anti-Stokes Emission Properties. The very weak emission bands around 412 nm (in the blue region of the spectrum), presented in Figure 2a, are assigned to a $^5G_5 \rightarrow {}^5I_8$ transition. The emission bands between 450 and 475 nm (Figures 2a,b) in the blue-green are assigned to the $^5G_6 \rightarrow {}^5I_8$ transition. The blue-green emission bands between 480 and 505 nm are attributed to the $^3K_8$, $^5F_3$, $^5F_2 \rightarrow {}^5I_8$ transitions (it should be noted that these three energy levels are close together on the Dieke diagram in Figure 1 and may be expected to overlap due to the splitting of each by the crystal field). The green emission bands in the range 505−520 nm will be assigned later in this article. The intense yellow-green emission bands from 530 to 570 nm (Figure 2c) are due to the $^5F_4 \rightarrow {}^5I_8$ and $^5S_2 \rightarrow {}^5I_8$ transitions (the $^5S_2$ and $^5F_4$ are treated as being closely spaced in energy in agreement with previous literature).[21,25] The fine structure between 580 and 595 nm (Figure 2c) on the low-energy side of the yellow-green peak may also be due to the last two transitions.

3.4. Anti-Stokes Raman Bands. The most intense anti-Stokes Raman band is centered at a Raman shift of 375 cm^{-1} from the laser line and is seen at 618 nm in Figure 2c.

3.5. Stokes Emission Properties. On the Stokes side of the spectrum the emission bands between 635 and 675 nm are due to the $^5F_5 \rightarrow {}^5I_8$ transition (see Figure 3a). The $^5F_5$ level is the state that is accessed by absorption of an initial photon of 632.8 nm light and thus the $^5F_5 \rightarrow {}^5I_8$ transition represents re-emission from this state.

There are some weak emission bands at 681−694 nm that will be discussed below, as will the emission manifold occurring between 740 and 780 nm (see Figure 3a).

The infrared emission bands between 870 and 895 nm are due to the $^5I_5 \rightarrow {}^5I_8$ transition (see Figure 3b).

3.6. Stokes Raman Bands. The main Stokes Raman band of cubic Y_2O_3 is at 375 cm^{-1} relative to the laser line and is seen at 643 nm in Figure 3a. The smaller Raman bands of cubic Y_2O_3 reported previously[1−4] are masked by the emission bands due to the $^5F_5 \rightarrow {}^5I_8$ transition.

3.7. Power Dependence Studies. Figure 4a presents a plot of the laser power dependence of the emission lines between 635 and 675 nm. Clearly the slope determined from the linear regression fit in Figure 4a indicates that the $^5F_5 \rightarrow {}^5I_8$ transition is due to a one-photon process. The laser power dependence of

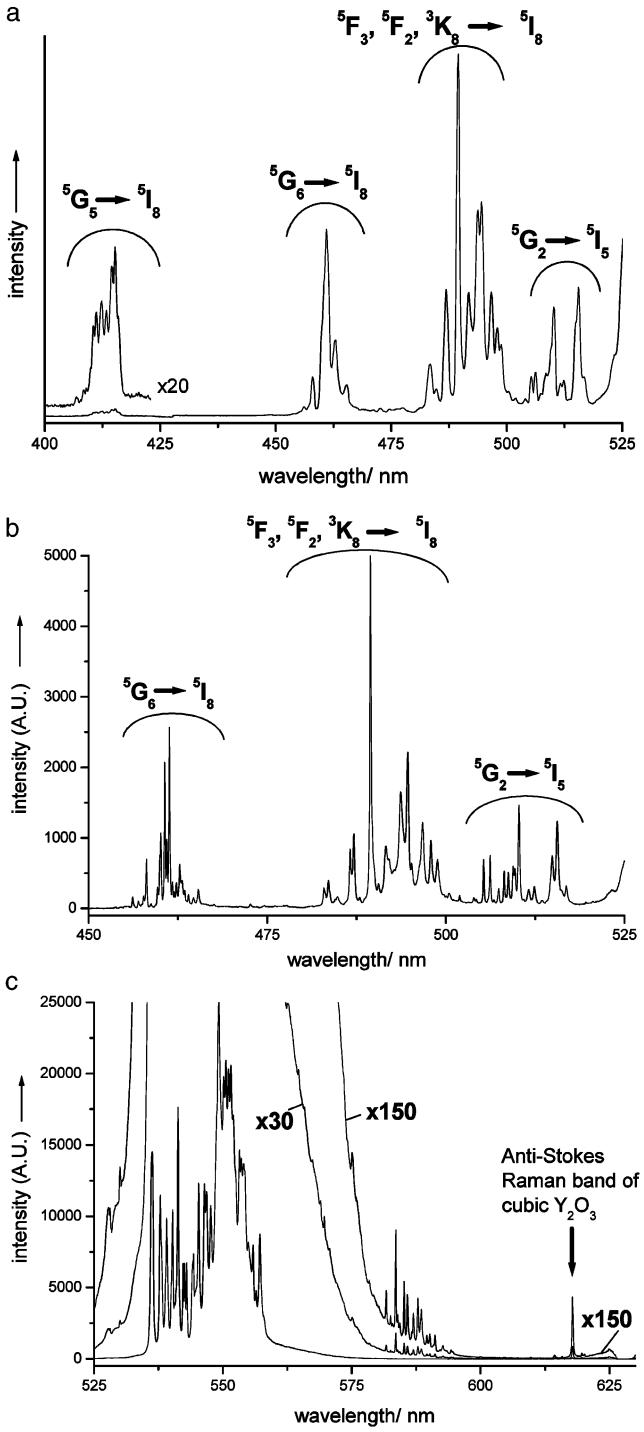

Figure 2. (a) Anti-Stokes emission spectrum of cubic Y_2O_3:Ho^{3+} (1 mol %) under 8 mW power of 632.8 nm excitation in the 400−525 nm range obtained at a temperature of 20 °C. This spectrum was obtained using a 600 g/mm grating. (b) Anti-Stokes emission spectrum of cubic Y_2O_3:Ho^{3+} (3 mol %) under 0.8 mW power of 632.8 nm excitation in the 450−525 nm range obtained at a temperature of 20 °C. This spectrum was obtained using a 1800 g/mm grating providing a linear reciprocal dispersion of 2 nm/mm. (c) Anti-Stokes emission spectrum of cubic Y_2O_3:Ho^{3+} (3 mol %) under 0.8 mW power of 632.8 nm excitation in the 525−630 nm range obtained at a temperature of 20 °C. The bands in the region from 525 to 595 nm are due to the $^5F_4 \rightarrow {}^5I_8$ and $^5S_2 \rightarrow {}^5I_8$ transitions. The anti-Stokes Raman band of cubic Y_2O_3 is marked by an arrow and appears at 618 nm (i.e., at a wavenumber displacement of −375 cm^{-1} from the 632.8 nm laser line).

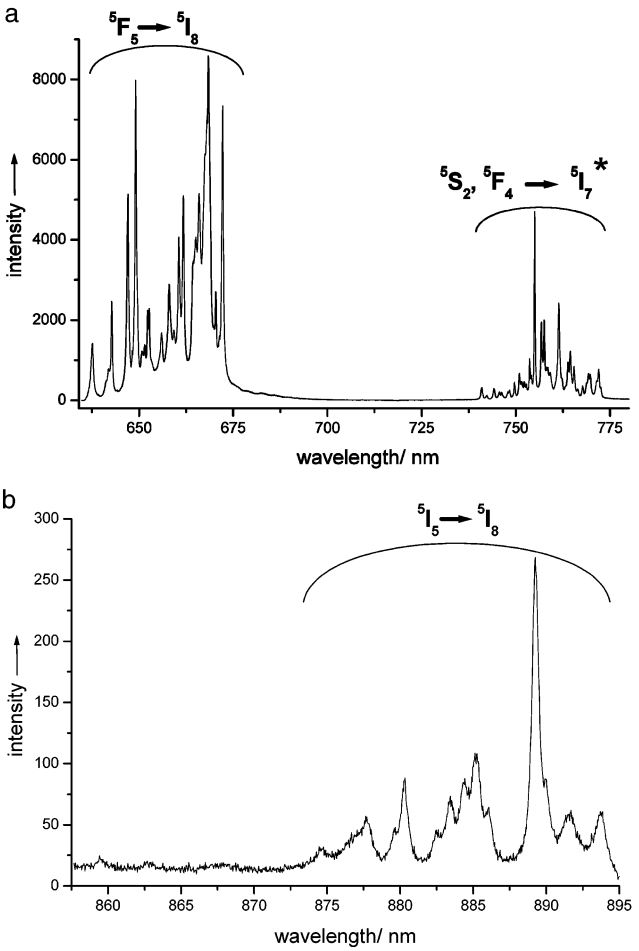

Figure 3. (a) Stokes emission spectrum of cubic Y_2O_3:Ho^{3+} (3 mol %) under 0.8 mW power of 632.8 nm excitation in the 635−780 nm range obtained at a temperature of 20 °C. The asterisk (*) indicates that this transition is re-assigned at the end of the discussion section of this article. (b) Stokes emission spectrum of cubic Y_2O_3:Ho^{3+} (10 mol %) under 8 mW power of 632.8 nm excitation, in the region 857−895 nm at a temperature of 20 °C.

the small emission bands in the 681−694 nm region (Figure 4b) shows that they arise from a process involving the absorption of two photons. From Figure 1 there are a number of transitions that could be responsible for these emissions. These include $^5G_2 \rightarrow {}^5F_5$, ? $\rightarrow {}^5I_4$ (? signifies a level that has not been assigned in the Dieke diagram, Figure 1), $^5G_5 \rightarrow {}^5I_6$ and $^5F_3 \rightarrow {}^5I_7$. It may be possible to rule out the $^5F_3$,$^5F_2$,$^3K_8 \rightarrow {}^5I_7$ transition, as this would be expected to have a similar photon dependence to the $^5F_3$,$^5F_2$,$^3K_8 \rightarrow {}^5I_8$ transition, which is discussed below.

In Figure 4c the power dependence of the 740−780 nm emission manifold is given. These bands have a photon dependence of 1.5. Thus it is interpreted that these bands originate from a state that is excited by a mechanism involving ESA (see Figure 1). Such an ESA process involves absorption of a 632.8 nm photon by Ho^{3+} in the $^5I_7$ state, promoting it to the $^5F_2$, $^3K_8$, or $^5F_3$ levels in agreement with the mechanism previously reported.[11] Decay from these last three levels to the $^5F_4$,$^5S_2$ levels occurs, followed by radiative decay to the $^5I_7$ level. These last two transitions, viz. the $^5F_4 \rightarrow {}^5I_7$ and the$^5S_2 \rightarrow {}^5I_7$ transitions, would be the emission that accounts for the 740−780 nm bands.

The power dependence of the main anti-Stokes emission bands between 530 and 570 nm (see Figure 1S in the Supporting Information) indicates that they also arise from a 1.5-photon process. The transitions $^5F_4 \rightarrow {}^5I_8$ and $^5S_2 \rightarrow {}^5I_8$ would account

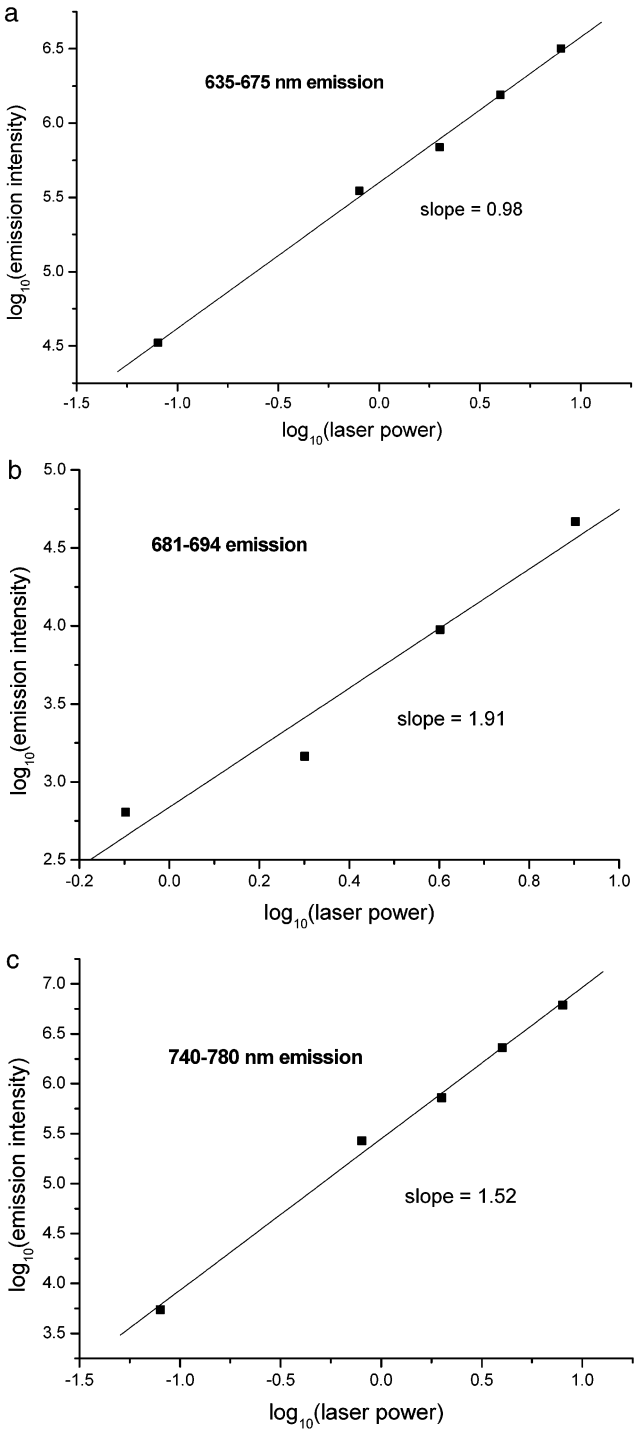

Figure 4. Power dependence of Stokes emission bands in the regions (a) 635−675 nm, (b) 681−694, and (c) 740−780 nm. These were determined from logarithmic plots of emission intensity versus laser power for laser exciting powers of 0.08, 0.8, 2, 4, and 8 mW in (a) and (c) and 0.8, 2, 4, and 8 mW for (b).

for these bands and would arise from the same ESA process discussed above. The $^5F_4$,$^5S_2 \rightarrow {}^5I_8$, and $^5F_4$,$^5S_2 \rightarrow {}^5I_7$ emissions arise from the same levels ($^5F_4$,$^5S_2$) once they are populated, requiring them to have similar photon dependences.

The other anti-Stokes bands were too weak to enable full power dependence studies to be carried out at this concentration of Ho^{3+}. However, the bands between 470 and 475 nm due to the $^5G_6 \rightarrow {}^5I_8$ transition showed a two-photon dependence on the exciting light as did the bands between 580 and 595 nm mentioned above. The likelihood as suggested earlier, is that

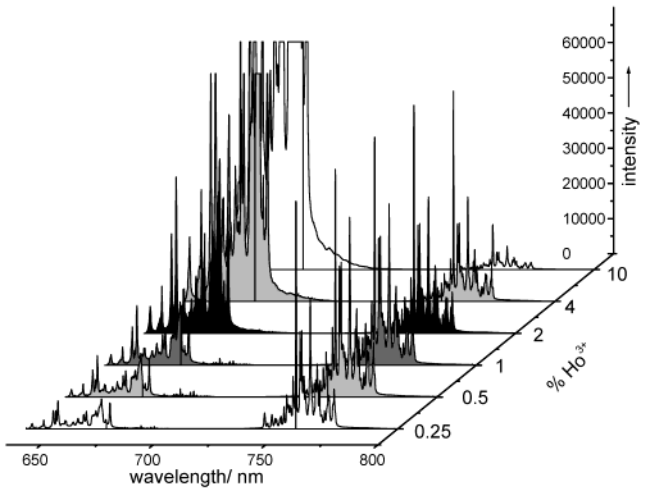

Figure 5. Stokes emission spectra excited by 8 mW power of 632.8 nm excitation in the range 635−800 nm plotted as a function of percentage Ho^{3+} in cubic Y_2O_3:Ho^{3+}.

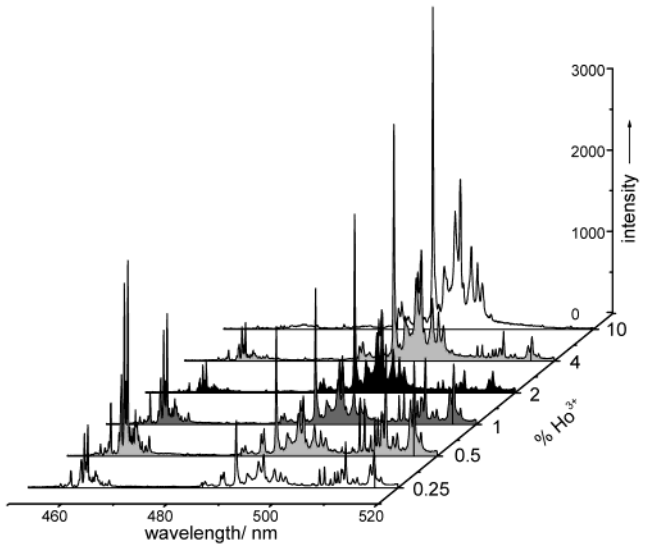

Figure 6. Anti-Stokes emission spectra excited by 8 mW power of 632.8 nm excitation in the range 450−520 nm plotted as a function of percentage Ho^{3+} in cubic Y_2O_3:Ho^{3+}.

these last bands are part of the transitions causing the main yellow-green emission. However, as will be seen below, the situation for these bands is not so straightforward. In addition, the bands between 505 and 520 nm show a two-photon dependence on the exciting light and would fit a $^5G_2 \rightarrow {}^5I_5$ transition. The $^5F_2$, $^3K_8$, and $^5F_3 \rightarrow {}^5I_8$ transitions, which give rise to the emission bands between 480 and 505 nm, all have a 1.6-photon dependence that can be explained at this concentration of Ho^{3+} by the ESA process from the $^5I_7$ level already discussed.[11] The blue emission band centered at 412 nm is due to the $^5G_5 \rightarrow {}^5I_8$ transition. It originates from the $^5G_2$ level, which would have to be populated by a sequential two-photon absorption process involving the $^5F_5$ level as an intermediate state. For other transitions that occur from the $^5G_5$ level, or from levels of lower energy, then the requirement is the absorption of one red photon and a second photon via an ESA mechanism from a state above or including the $^5I_6$ state. The ESA processes are also indicated in Figure 1.

3.8. Concentration Studies and Dilution. When the amount of Ho^{3+} was increased from 0.5 to 10 mol % Ho^{3+}, the intensity of some of the emission bands changed dramatically. The bands that manifested the greatest change were those most dependent on cross-relaxation processes (see below), which increased as the $Ho^{3+}-Ho^{3+}$ distances decreased. The Ho^{3+} concentration dependence is shown in the emission spectra in Figures 5 and 6 and in Figure 2S of the Supporting Information.

In Figure 5 the concentration dependence of the bands in the 635−800 nm range are displayed. As set out above, there are three main transitions that account for these bands. First the bands between 635 and 675 nm that arise from the $^5F_5 \rightarrow {}^5I_8$ emission (due to a one-photon absorption process) increase dramatically with concentration as the main upconversion bands (shown in Figure 2S in the Supporting Information) decrease from their highest levels in the 0.5% Ho^{3+} sample. It should be noted that the weak emission bands between 681 and 694 nm also maximize at a concentration of 0.5% Ho^{3+} and are not discernible in the spectrum of the sample containing 10 mol % Ho^{3+}. Similarly, the emission intensities of the bands between 740 and 780 nm (also shown in Figure 5), which maximize at 0.5% Ho^{3+} (and are due to a photon dependence of 1.5), also diminish as the concentration increases.

In Figure 6, the Ho^{3+} concentration dependences in the region 450−520 nm are presented. Three sets of bands can clearly be seen, two of which maximize at 0.5% Ho^{3+} and fall away down to 10%, whereas the third that occurs between 480 and 505 nm increases with Ho^{3+} concentration. This set of bands that arise from the $^3K_8$, $^5F_3$, $^5F_2 \rightarrow {}^5I_8$ transitions, which we ascribed to an ESA process at low Ho^{3+} concentration, clearly shows a concentration dependence that cannot be explained by such processes at the higher Ho^{3+} concentrations. The minimum ESA process would have involved the absorption of a red 632.8 nm photon by a Ho^{3+} ion in the $^5I_7$ state. An alternative way that this emission band can arise and show the concentration dependence observed would be via cross-relaxation involving two Ho^{3+} cations, one in the metastable $^5I_7$ state and the other in the $^5F_5$ state. This would then produce one in an excited state corresponding to the $^3K_8$, $^5F_3$, $^5F_2$ levels and the other in the ground state corresponding to the ($^5F_5$, $^5I_7 \rightarrow \{^3K_8, {}^5F_3, {}^5F_2\}$, $^5I_8$) transition (see Figure 1 where this cross-relaxation process is included).[11,39] A photon dependence of 1.6 for the $^3K_8$, $^5F_3$, $^5F_2 \rightarrow {}^5I_8$ transition was measured from a power dependence study of the 10% Ho^{3+} concentration, as shown in Figure 3S in the Supporting Information.

In Figure 4S in the Supporting Information the concentration dependence of the bands in the 580−600 nm region is presented. The intensity changes are clearly complex. To gain insight into the origins of the emissions, we plotted the intensities of four of the emission bands as a function of concentration and we present these plots in Figure 7. Clearly the behavior of the 530−570 nm band (due to the $^5F_4 \rightarrow {}^5I_8$ and $^5S_2 \rightarrow {}^5I_8$ transitions) and the 735−780 nm band (due to the $^5F_4 \rightarrow {}^5I_7$ and $^5S_2 \rightarrow {}^5I_7$ transitions) are the same, as expected for transitions originating from the same level as mentioned earlier. The behavior of the 480−505 nm band (due to the $^3K_8$, $^5F_3$, $^5F_2 \rightarrow {}^5I_8$ transitions) clearly increases with concentration, as discussed in the text above. The 577−600 nm band shows an intermediate trend between these two kinds of behavior. Clearly this means that two processes are involved in the emissions of this band. The first maximizes at 0.5 mol % Ho^{3+} and arises from a two-photon process. The second, however, increases with increasing concentration and is ascribed to a cross-relaxation process similar to that indicated in Figure 1 but involving the $^5I_4$ state rather than the $^5F_5$ state (see below). The fact that this band is weak and is seen to longer wavelength than the 530−570 nm band is taken as evidence that the $^5S_2$ and $^5F_4$ levels that are usually displayed as coinciding in low-resolution studies are in fact

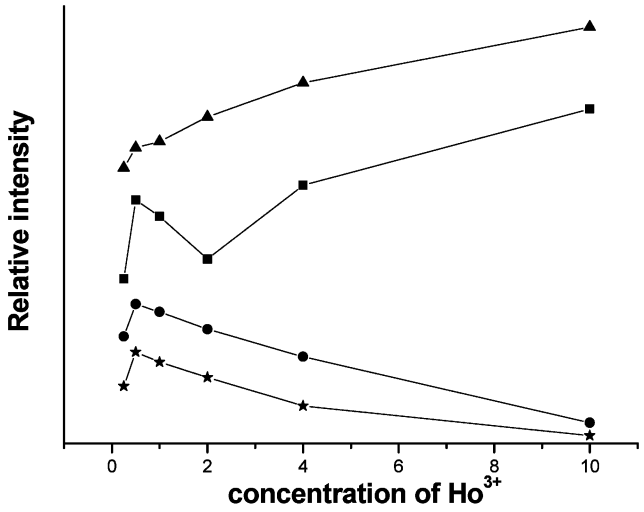

Figure 7. Behaviors of the 530−570 nm (★), 577−600 nm (■), 735−780 nm (●), and 480−505 nm (▲) emission bands as a function of the Ho^{3+} concentration. The relative emission intensities of each band are plotted as a function of concentration but are not scaled relative to each other.

discrete levels and this is why the behavior of this band is different to the 530−570 nm band. Further evidence for this splitting comes from careful examination of the 740−780 nm band. This shows a set of bands in the 800 nm region that are of even lower intensity than the 577−600 nm band. These bands are shown in Figure 5S in the Supporting Information and could arise from a second cross-relaxation process involving the $^5I_4$ level, which is a dark state in the main processes but which can receive energy from another Ho^{3+} ion via the $^5I_7 \rightarrow {}^5I_8$ transition raising it to the $^5S_2$ level. The concentration behavior of the bands around 800 nm is not the same as those in the 577−600 nm band in that they are nearly absent in the 10 mol % Ho^{3+} sample. However, as the $^5I_4$ level is a dark state and the energy entering the $^5F_4$ level gives rise to the $^5F_4 \rightarrow {}^5I_8$ (between 577 and 600 nm) transition as well as the $^5F_4 \rightarrow {}^5I_7$ transition and the fact that the latter transition could also populate other Ho^{3+} ions up to the $^5I_4$ state would account for the lack of intensity of this band at the high concentration. This would of course mean that the previously discussed strong green emission from the $^5F_4$,$^5S_2 \rightarrow {}^5I_8$ and the near-infrared emission from the $^5F_4$,$^5S_2 \rightarrow {}^5I_7$ should actually be assigned to $^5F_4 \rightarrow {}^5I_8$ and $^5F_4 \rightarrow {}^5I_7$ transitions.

There is some evidence in the literature to support our discrimination between emission bands due to transitions from the $^5F_4$ and $^5S_2$ states.[33,34] Patel et al.[34] label a band at 538.3 nm in the absorption spectrum of $Lu_3Al_5O_{12}:Ho^{3+}$ (Figure 1 in ref 34) as being due to the $^5I_8 \rightarrow {}^5F_4$ transition of Ho^{3+} and a weaker band at 549.4 nm as being due to the $^5I_8 \rightarrow {}^5S_2$ transition. Their assignments are supported by calculations that predict that these bands have absorption cross-sections of 3.820×10^{-22} and 2.374×10^{-22} cm^2, which are in reasonably good agreement with experimentally determined values of 3.785×10^{-22} and 2.308×10^{-22} cm^2, respectively. The predicted average wavelengths of the emission bands due to the $^5F_4 \rightarrow {}^5I_8$ and $^5S_2 \rightarrow {}^5I_8$ transitions were at 538.4 and 548.1 nm, whereas those due to the $^5F_4 \rightarrow {}^5I_7$ and $^5S_2 \rightarrow {}^5I_7$ transitions were at 750.6 and 769.6 nm, respectively. From the foregoing, it can be seen that there is a greater predicted difference in wavelength between the bands due to the $^5F_4 \rightarrow {}^5I_7$ and $^5S_2 \rightarrow {}^5I_7$ transitions (19.0 nm) than between those due to the $^5F_4 \rightarrow {}^5I_8$ and $^5S_2 \rightarrow {}^5I_8$ transitions (9.7 nm).

In a study of $CaF_2:Ho^{3+}$, the predicted average wavelengths of the emission bands due to the $^5F_4 \rightarrow {}^5I_8$ and $^5S_2 \rightarrow {}^5I_8$ transitions were at 539.4 and 543.5 nm, respectively, whereas the average wavelengths of those due to the $^5F_4 \rightarrow {}^5I_7$ and $^5S_2 \rightarrow {}^5I_7$ transitions were at 742.2 and 750.9 nm, respectively.[33] Again, it can be seen that there is a greater predicted wavelength difference between the bands due to the $^5F_4 \rightarrow {}^5I_7$ and $^5S_2 \rightarrow {}^5I_7$ transitions (8.7 nm) than between those due to the $^5F_4 \rightarrow {}^5I_8$ and $^5S_2 \rightarrow {}^5I_8$ transitions (4.1 nm), although it should be noted that these wavelength differences are smaller in the CaF_2 lattice than in $Lu_3Al_5O_{12}$, which would be in keeping with a weaker crystal field in the former.

The average wavelengths of the emission bands due to the $^5F_4 \rightarrow {}^5I_8$ and $^5S_2 \rightarrow {}^5I_8$ transitions observed in this work for cubic $Y_2O_3:Ho^{3+}$ are 550 and 584 nm, respectively, giving a difference of 34 nm. Also, the average wavelengths of the emission bands due to the $^5F_4 \rightarrow {}^5I_7$ and $^5S_2 \rightarrow {}^5I_7$ transitions are 758 and 800 nm, respectively, giving a difference of 42 nm. The reason for the larger differences in wavelength in cubic $Y_2O_3:Ho^{3+}$ is due to the high crystal field strength for the C_2 sites of the cubic Y_2O_3 lattice.

It is noteworthy that the predicted differences between the wavelength locations of emission bands due to the transitions from the $^5F_4$ and $^5S_2$ states down to the $^5I_7$ state are larger than those down to the $^5I_8$ ground state.[33,34] This is consistent with our experimental observations of the wavelength locations of these emission bands.

4. Conclusions

The anti-Stokes emission properties of cubic $Y_2O_3:Ho^{3+}$ have been studied in the concentration range 0.25−10 mol % Ho^{3+}. Maximum upconversion emission for the main yellow-green emission in the range 530−570 nm is observed at a concentration of 0.5% under 632.8 nm excitation. At high concentrations of Ho^{3+} where this yellow-green emission is less efficient, bands in the 480−505 nm region increase in relative intensity and these originate from a mechanism that is herein shown to involve concentration dependent cross-relaxation of Ho^{3+} cations in agreement with the findings of Pouradier and Auzel.[11] All features of the emission spectra of cubic $Y_2O_3:Ho^{3+}$ excited by 632.8 nm light have been ascribed.

This work has allowed us to discriminate between emission bands due to transitions originating from the $^5F_4$ and $^5S_2$ levels. Those originating from the $^5F_4$ level (viz. the yellow-green 530−570 nm and the near-infrared 740−780 nm bands) were measured to have a similar photon dependence.

Acknowledgment. We express our gratitude to the EPSRC (grant ref. nos. GR/L85176, GR/M78847 and GR/N28535). We also thank one of the referees for drawing to our attention the importance of ref 11, which has not been given the attention it deserves in the literature.

Supporting Information Available: Figure 1S: Power dependence of the yellow-green anti-Stokes emission band in the region 530−570 nm. This was determined from a logarithmic plot of emission intensity versus laser power for laser exciting powers of 0.08, 0.8, 2, 4, and 8 mW. Figure 2S: Anti-Stokes emission spectra excited by 0.8 mW power of 632.8 nm excitation in the range 425−630 nm plotted as a function of percentage Ho^{3+} in cubic $Y_2O_3:Ho^{3+}$. Figure 3S: Power dependence of the anti-Stokes emission band in the region 480−505 nm. This was determined from a logarithmic plot of emission intensity versus laser power for laser exciting powers

of 0.8, 2, 4, and 8 mW. Figure 4S: Anti-Stokes emission spectra excited by 8 mW power of 632.8 nm excitation in the range 580−600 nm plotted as a function of percentage Ho^{3+} in cubic Y_2O_3:Ho^{3+}. Figure 5S: Stokes emission spectrum of cubic Y_2O_3:Ho^{3+} (3 mol %) under 8 mW power of 632.8 nm excitation in the 730−830 nm range obtained at a temperature of 20 °C. The $^5F_4 \rightarrow {}^5I_7$ transition is shown next to the $^5S_2 \rightarrow {}^5I_7$ transition. This information is available free of charge via the Internet at http://pubs.acs.org.

References and Notes

(1) Silver, J.; Martinez-Rubio, M. I.; Ireland, T. G.; Fern, G. R.; Withnall, R. *J. Phys. Chem. B* **2001**, *105*, 948.
(2) Silver, J.; Martinez-Rubio, M. I.; Ireland, T. G.; Withnall, R. *J. Phys. Chem. B* **2001,** *105*, 7200.
(3) Silver, J.; Martinez-Rubio, M. I.; Ireland, T. G.; Fern, G. R.; Withnall, R. *J. Phys. Chem. B.* **2001**, *105*, 9107.
(4) Silver, J.; Martinez-Rubio, M. I.; Ireland, T. G.; Fern, G. R.; Withnall, R. *J. Phys. Chem. B* **2003**, *107*, 1548.
(5) Vecht, A.; Gibbons, C.; Davies, D.; Jing, X.; Marsh, P.; Ireland, T. G.; Silver, J.; Newport. A. *J. Vac. Sci., Technol. B* **1999**, *17*, 750.
(6) Vecht, A.; Jing, X.; Gibbons, C.; Ireland, T. G.; Davies, D.; Marsh, P.; Newport A. *SID Technol. Dig.* **1998**, *29*, 1043.
(7) Jing, X.; T. G. Ireland, T. G.; Gibbons, C.; Barber, D. J.; Silver, J.; Vecht, A.; Fern, G. R.; Trogwa, P.; Morton, D. *J. Electrochem. Soc*. **1999**. *146*, 4564.
(8) Martinez-Rubio, M. I.; Ireland, T. G.; Fern, G. R.; Silver, J.; Vecht A. *J. Electrochem. Solid State Lett.* **2000**, *3*, 446.
(9) Martinez-Rubio, M. I.; Ireland, T. G.; Fern, G. R.; Silver, J.; Snowden M. J. *Langmuir* **2001**, *17*, 7145.
(10) Silver, J.; Galliano, R. I.; Fern G. R.; Ireland, T. G.; Vecht A.; Withnall R. *SID Digest Tech. Pap.* **2002**, *33*, 20.
(11) Pouradier, J. F.; Auzel, F. *J. Phys.* **1976**, *37*, 421.
(12) Johnson, L. F.; Guggenheim, H. *Appl. Phys. Lett.* **1971**, *19*, 44.
(13) Allain, J. Y.; Monerie, M.; Poignant, H. *Electron. Lett.* **1990**, *26*, 261.
(14) Funk, D. S.; Eden, J. G. *IEEE J. Sel. Top. Quantum Electron.* **1995**, *1*, 784.
(15) Funk, D. S.; Stevens, S. B.; Wu, S. S.; Eden, J. G. *IEEE J. Quantum Electron.* **1996**, *32*, 638.
(16) Chivian, J.; Case, W.; Eden, D. *Appl. Phys. Lett.* **1979**, *35*, 124.
(17) Lenth, W.; Macfarlane, R. M. *J. Lumin.* **1990**, *45*, 346.
(18) Malinowski, M.; Pirimadowicz, R.; Frukacz, Z.; Chadeyron, G.; Mahiou, R.; Joubert, M. F. *Opt. Mater.* **1999**, *12*, 409.
(19) Joubert, M. F.; Guy, S.; Malinowski, M.; Pirimadowicz, R.; Wnuk, A.; Chadeyron, G. *Radiation Eff. Def. Solids* **1999**, *150*, 79.
(20) Liu, G. K.; Chen, Y. H.; Beitz, J. V. *J. Lumin.* **1999**, *81*, 7.
(21) Kück, S.; Sokólska, I. *Chem. Phys. Lett.* **2000**, *325*, 257.
(22) Malinowski, M.; Wnuk, A.; Frukacz, Z.; Chadeyron, G.; Mahiou, R.; Guy, S.; Joubert, M. F. *J. Alloys Compounds* **2001**, *323*−*324*, 731.
(23) Ashurov, M. K.; Yu, K.; Zarikov, E. W.; Kaminskii, A. A.; Osiko, V. V.; Sobol, A. A.; Timoshechkin, M. I.; Fedorov, W. A.; Szabaltai, A. A. *Neorg Mater.* **1979**, *15*, 1250.
(24) Gruber, J. B.; Hills, M. J.; Seltzer, M. D.; Stevens, S. B.; Morrison, C. A.; Turner, G. A.; Kokta, M. R. *J. Appl. Phys.* **1991**, *69*, 8183.
(25) Malinowski, M.; Frukacz, Z.; Szuflinska, M.; Wnuk, A.; Kaczkan, M. *J. Alloys Compounds* **2000**, *300*−*301*, 389.
(26) Shaw, L. B.; Chang, R. S.; Djeu, N. *Phys. Rev. B* **1994,** *50*, 6609.
(27) Tang, S. H.; Zhang, H. Y.; Kuok, M. H.; Kee, S. C. *Phys. Stat. Solidi B* **1991**, *168*, 351.
(28) Zhang, X.; Jouart, J. P.; Mary, G. *J. Phys. Condens. Mater*. **1998**, *10*, 493.
(29) Zhang, X.; Liu, X.; Jouart, J. P.; Mary, G. *Chem. Phys. Lett.* **1998**, *287*, 659.
(30) Zhang, X.; Liu, X.; Jouart, J. P.; Mary, G. *J. Lumin.* **1998**, *78*, 289.
(31) Zhang, X.; Jouart, J. P.; Bouffard, M.; Mary, G. *Phys. Stat. Solidi B* **1994**, *184*, 559.
(32) Reddy, B. R.; Nash-Stevenson, S.; Venkateswarlu, P. *J. Opt. Soc. Am. B* **1994**, *11*, 923.
(33) Bullock, S. R.; Reddy, B. R.; Venkateswarlu, P.; Nash-Stevenson, S. *J. Opt. Soc. Am. B* **1997**, *14*, 553.
(34) Patel, D. N.; Reddy, B. R.; Nash-Stevenson, S. *Opt. Mater*. **1998**, *10*, 225.
(35) Müller, P.; Wermuth, M.; Güdel, H. U. *Chem. Phys. Lett.* **1998**, *290*, 105.
(36) Mosses, R. W.; Wells, J.-P. R.; Gallagher, H. G.; Han, T. P. J.; Yamaga, M.; Kodama, N.; Yosida, T. *Chem. Phys. Lett.* **1998**, *286*, 291.
(37) Matijevic, E.; Hsu, W. P. *J. Colloid Interface Sci*. **1987**, *118*, 506.
(38) Akinc, M.; Sordelet, D. *J. Colloid Interface Sci*. **1988**, *122*, 47.
(39) Auzel, F.; Chen, Y. *J. Lumin.* **1995**, *65*, 45.